

# Properties of heavy rare-gases adlayers on graphene substrates

Lucas Madeira<sup>1,\*</sup> and Silvio A. Vitiello<sup>2</sup>

<sup>1</sup>*Department of Physics and Astronomy, Arizona State University, Tempe, Arizona 85287, USA*

<sup>2</sup>*Instituto de Física Gleb Wataghin, Universidade Estadual de Campinas, UNICAMP, Campinas 13083-859, Brazil*

(Dated: August 10, 2021)

We investigated properties of heavy rare-gases, Ne, Ar, Kr, Xe and Rn, adsorbed on graphene substrates using molecular dynamics. We gathered evidences of commensurate solids for Ne and Kr adlayers, one of them is given by a typical behavior of the nearest neighbor distance of the adatoms. The specific heat and the melting temperature were calculated and both indicate continuous melting for all heavy noble-gases studied. We also determined the distance between the adlayer and the substrate.

PACS numbers: 68.43.-h, 64.70.dj

## I. INTRODUCTION

The study of adsorption on solid surfaces began long ago because of its intrinsic scientific interest and also because of its importance as a mean to improve the understanding of physical processes at atomic level, which can be of technological interest. Thin films adsorbed on substrates are confined to a narrow domain near the surface of the substrate, and they are very close to a two-dimensional (2D) phase of matter. The subject of adsorbed layers of a given material is particularly interesting because of possible bidimensional phases that have no tridimensional analog. Furthermore, the spatial periodicity of the substrate may cause interesting effects when the adsorbate lattice “feels” the symmetry of the substrate. Usually, the density distribution and other thermodynamical properties are quite different from what would be expected from a simple 2D material not adsorbed in a substrate.

Although the adsorption of noble gases on graphite substrates has been extensively studied from the theoretical and experimental point of view (for a comprehensive review of the subject the reader is referred to Ref. 1 and references therein), the physics of noble gases on graphene has not received the same attention. It is our intention to extend this large body of knowledge by studying properties of heavy noble gases adsorbed on graphene substrates, a system that presents remarkable novel properties when compared with graphite.

Noble gases adsorbed on graphite present interesting properties and we restrict ourselves to cite and compare some of the most remarkable of them with our object of study. The Ne adsorbed on graphite exhibits a superlattice structure<sup>2</sup> known as  $\sqrt{7} \times \sqrt{7}$ , whereas Kr and Xe form a  $\sqrt{3} \times \sqrt{3}$  commensurate lattice<sup>3</sup>. For Ar on graphite the order of the melting transition is unsettled, due to the observation of two peaks in specific heat measurements of the system<sup>4,5</sup>. Radon is set apart from the other noble gases because it is radioactive. Although there is great interest in Rn filters, which requires knowledge of adsorption behavior on solid surfaces, little is known about Rn adsorbed on graphite<sup>6</sup>.

This work is organized as follows. In the next section, we present the methods employed in our work. Section III contains our results, in subsection A we discuss the spatial distribution of the adatoms. We have observed evidences of Ne  $\sqrt{7} \times \sqrt{7}$  and Kr  $\sqrt{3} \times \sqrt{3}$  commensurate solids. For the other noble gases, the adlayer is incommensurate with the graphene substrate for the temperature and densities ranges considered. The specific heats are calculated in subsection B and the melting temperatures of the adlayers are determined in subsection C, both properties present evidences of a continuous melting for all heavy rare-gases studied. We also estimated two other properties of the adlayers: the first neighbor distance, subsection D, and the distance between the adlayer and the substrate, in subsection E. We note that it is possible to relate the behavior of these quantities directly to the specific heat peaks or the melting transition. It is also noteworthy that the commensurate adlayers have a typical behavior of the nearest neighbor spacing near the melting transition. The discussion of the results and conclusions are presented in Section IV.

## II. METHODS

In this section we start by briefly introducing the two commensurate structures,  $\sqrt{3} \times \sqrt{3}$  and  $\sqrt{7} \times \sqrt{7}$ . The adopted potential interactions are presented in subsection B. In subsection C we give some details of the simulations.

### A. Commensurate structures

The usual primitive and basis vectors provide a convenient way of expressing the periodicity of both substrate and adlayer lattices. The graphene sheet is a triangular lattice with a basis of two carbon atoms at

$$\mathbf{b}_1 = \frac{(\mathbf{a}_1 + \mathbf{a}_2)}{3} = b \hat{\mathbf{x}}, \quad \mathbf{b}_2 = 2\mathbf{b}_1 = 2b \hat{\mathbf{x}}, \quad (1)$$

where  $b$  is the bond length of two carbon atoms assumed to be 1.42 Å and  $\mathbf{a}_1$  and  $\mathbf{a}_2$  are primitive vectors of the

2D Bravais lattice of the triangular, or hexagonal close-packed structure,

$$\mathbf{a}_1 = a \left( \frac{\sqrt{3}}{2} \hat{\mathbf{x}} + \frac{1}{2} \hat{\mathbf{y}} \right), \quad \mathbf{a}_2 = a \left( \frac{\sqrt{3}}{2} \hat{\mathbf{x}} - \frac{1}{2} \hat{\mathbf{y}} \right). \quad (2)$$

The so called  $\sqrt{3} \times \sqrt{3}R30^\circ$  adlayer commensurate structure is a triangular lattice of constant  $3b$  and axes rotated by  $30^\circ$  relative to the underlying triangular lattice. The  $\sqrt{3} \times \sqrt{3}R30^\circ$  primitive vectors  $\mathbf{c}_1$  and  $\mathbf{c}_2$  are obtained from Eq. (2),

$$\mathbf{c}_1 = 3b\hat{\mathbf{x}}, \quad \mathbf{c}_2 = \frac{3b}{2}\hat{\mathbf{x}} + \frac{3b\sqrt{3}}{2}\hat{\mathbf{y}}, \quad (3)$$

with the identification  $a = 3b$ .

The structure  $\sqrt{7} \times \sqrt{7}R19.1^\circ$ , Fig. 1, is a superlattice with primitive vectors

$$\mathbf{d}_1 = \mathbf{a}_1 + 2\mathbf{a}_2, \quad \mathbf{d}_2 = 3\mathbf{a}_2 - 2\mathbf{a}_1, \quad (4)$$

and four atoms in the basis, one at a superlattice site, the origin, and three atoms at

$$\mathbf{f}_1 = \frac{\mathbf{d}_1}{2}, \quad \mathbf{f}_2 = \frac{\mathbf{d}_2}{2}, \quad \mathbf{f}_3 = \frac{\mathbf{d}_1 + \mathbf{d}_2}{2}. \quad (5)$$

Notice that  $|\mathbf{d}_1| = |\mathbf{d}_2| = a\sqrt{7}$ , and the angle between the vectors  $\mathbf{d}_1$  and  $\mathbf{a}_1$  is  $19.1^\circ$ , hence the terminology  $\sqrt{7} \times \sqrt{7}R19.1^\circ$ .

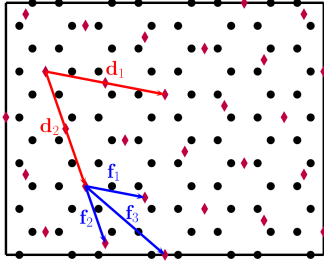


FIG. 1. (Color online) Commensurate  $\sqrt{7} \times \sqrt{7}R19.1^\circ$  lattice denoted by diamonds ( $\blacklozenge$ ), the circles ( $\bullet$ ) stand for the graphene honeycomb lattice. Vectors  $\mathbf{d}_i$  and  $\mathbf{f}_i$  are defined in Eq. (4) and Eq. (5), respectively

## B. Interacting potentials

The total potential energy of each system formed from the noble gases atoms X, (X=Ne, Ar, Kr, Xe or Rn), we have considered is given by

$$U_X = \sum_{i < j}^{N_X} V_X(r_{ij}) + \sum_i^{N_X} \sum_j^{N_C} V_{X-C}(r_{ij}) + \sum_{i,j,k}^{N_C} V_{ijk}, \quad (6)$$

where  $N_X$  is the number of atoms of a given noble gas X,  $N_C$  is the number of carbon atoms in the substrate,  $r_{ij} = |\vec{r}_i - \vec{r}_j|$  and  $\vec{r}_i$  is the position of the  $i$ -th atom. The

first term on the right-hand side of Eq. (6) describes the pair interaction of atoms X of the adlayer, the second, the interaction of X with the substrate. The last term models interactions between the carbon atoms of the substrate.  $V_{ijk}$  is related to the Tersoff potential<sup>7-9</sup> which takes into account not only two-body interactions but also those of three-body among the carbon atoms in the substrate.

The pair interactions  $V_X$  we use between the adatoms give an accurate description of their potential energies. The potential depth and the position of the minimum increase with increasing atomic number, as illustrated in Fig. 2.

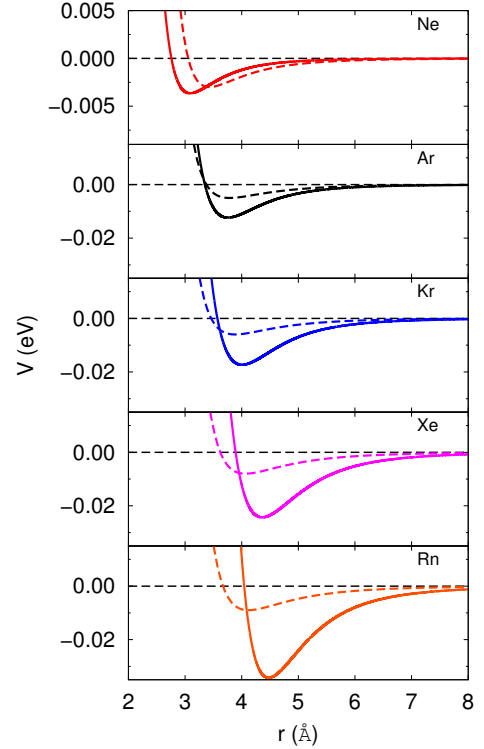


FIG. 2. (Color online)  $V_X$  (solid curves) and  $V_{X-C}$  (dashed curves) pair interaction energies. The Ne-Ne, Kr-Kr and Xe-Xe curves are for the interatomic potential HFD-B<sup>10-12</sup>; the Ar-Ar interactions is given by the HFDID1 potential<sup>13</sup>; the Rn-Rn interactions were based on the Tang-Toennies potential<sup>14</sup>.  $V_{X-C}$  is a LJ potential for the Ne-C, Ar-C, Kr-C, Xe-C and Rn-C interactions with the parameters of Table I.

The pairwise interaction we employ between an adsorbate atom X and the substrate carbon atoms,  $V_{X-C}$  in Eq. (6), is modeled by a Lennard-Jones (LJ) potential

$$V_{X-C}(r_{ij}) = 4\epsilon_{XC} \left[ \left( \frac{\sigma_{XC}}{r_{ij}} \right)^{12} - \left( \frac{\sigma_{XC}}{r_{ij}} \right)^6 \right], \quad (7)$$

where the parameters of the mixed pair X-C is obtained

TABLE I. Parameters of the Lennard-Jones interaction for the given X atoms displayed in the lines of the table,  $r$  values where  $V_X(r)$  and  $V_{X-C}(r)$  are minima are denoted by  $r_X^{(\min)}$  and  $r_{XC}^{(\min)}$ , respectively.

	$\sigma_X$ (Å)	$\epsilon_X$ (eV)	$r_X^{(\min)}$ (Å)	$\sigma_{XC}$ (Å)	$\epsilon_{XC}$ (eV)	$r_{XC}^{(\min)}$ (Å)
Ne <sup>10</sup>	2.759	0.0036	3.091	3.055	0.003	3.429
Ar <sup>13</sup>	3.400	0.0103	3.757	3.375	0.005	3.788
Kr <sup>11</sup>	3.571	0.0173	4.008	3.460	0.006	3.884
Xe <sup>12</sup>	3.892	0.0243	4.363	3.621	0.008	4.064
Rn <sup>14</sup>	3.988	0.0343	4.477	3.669	0.009	4.118

by combining rules<sup>1</sup> of the X and C atom pairs

$$\begin{aligned}\sigma_{XC} &= \frac{(\sigma_X + \sigma_C)}{2}, \\ \epsilon_{XC} &= \sqrt{\epsilon_X \epsilon_C}.\end{aligned}\quad (8)$$

The chosen carbon-carbon LJ parameters<sup>15</sup> are  $\sigma_C = 3.35$  Å and  $\epsilon_C = 0.0024$  eV. Table I summarizes  $\sigma_X$  and  $\epsilon_X$  from the literature, as well as the obtained X-C parameters. The corresponding LJ potential energies for the X-C pairs are plotted in Fig. 2. We note that the interactions between adatoms and the substrate (X-C) are much weaker than the one for the noble gases atoms (X-X), except for Ne.

### C. Simulation setup

Properties of the noble gases adsorbed on graphene systems were determined using molecular dynamics (MD) in the canonical ( $NVT$ ) ensemble. This classical approach is well-suited for heavy noble gases, with the possible exception of Ne, where quantum effects might affect some of the properties in which we are interested. Nevertheless we will disregard any quantum effect the Ne system might present.

Thermal averages of physical quantities were formed from as many as  $10^7$  time steps of 1 fs. In the presented study the LAMMPS (Large-scale Atomic/Molecular Massively Parallel Simulator)<sup>16</sup> code was used.

The initial positions of the atoms must be chosen carefully. The two dimensional unit cell of the  $\sqrt{3} \times \sqrt{3}R30^\circ$  commensurate lattice corresponds to 12 carbon atoms and 2 heavy noble gases atoms, as shown in Fig. 3. The lengths of the cell are  $L_x = 3\sqrt{3}b$  and  $L_y = 3b$ . The surface density  $\rho$  will be given hereafter in units of  $\rho_0 = 0.0636$  atoms/Å<sup>2</sup>, the density of the  $\sqrt{3} \times \sqrt{3}$  commensurate lattice. The initial  $z$  coordinate of the noble gases atoms is set as the minimum of the X-C pair potential.

Initial positions using the  $\sqrt{7} \times \sqrt{7}$  superlattice can be achieved with a cell of 224 X atoms and 784 C atoms, with corresponding superficial density of  $\rho = 1.71$ . Densities other than those of the two commensurate structures were initialized with triangular lattices with suitable lattice parameters. Tab. II summarizes the numbers of noble gases and carbon atoms and corresponding densities employed in the simulations. We use periodic

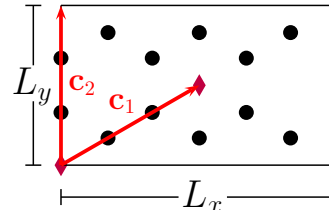


FIG. 3. (Color online) Commensurate lattice  $\sqrt{3} \times \sqrt{3}R30^\circ$  unit cell. The circles ( $\bullet$ ) represent the position of C atoms, diamonds ( $\blacklozenge$ ) indicate the position of the heavy noble gases atoms, we also plot the primitive vectors of Eq. (3).

TABLE II. Densities, number of noble gases atoms  $N_X$ , and carbon atoms  $N_C$  used in the simulations.

$\rho$	$N_X$	$N_C$
0.38	210	3360
0.73	232	1920
1.00	224	1344
1.08	216	1200
1.71	224	784

boundary conditions (PBC) in the  $xy$  plane of the substrate and the  $z$  coordinates of the carbon atoms were kept fixed. No PBC were employed in the  $z$  direction, normal to the substrate, in order to allow evaporation of noble gases atoms. Because the adlayer may be incommensurate with the substrate symmetry, we chose certain surface densities which guarantee the adatoms in a triangular lattice. The initial velocities were chosen from a Gaussian distribution compatible with the desired temperature.

## III. RESULTS

Our results are mainly for Ar/graphene systems, which was motivated in part by the interesting behavior of the relate system Ar/graphite. We studied properties at four Ar surface densities; at  $\rho = 1$  that in our units corresponds to an adlayer in the  $\sqrt{3} \times \sqrt{3}$  commensurate lattice, one slightly above this value, at  $\rho = 1.08$ , and two below:  $\rho = 0.73$  and  $0.38$ . Since the system Ne/graphite exhibits the superlattice  $\sqrt{7} \times \sqrt{7}$ , we also considered for our Ne/graphene system the corresponding density *i.e.*,  $\rho = 1.71$ , in addition to  $\rho = 1$ . For Xe, Kr and Rn we

restricted ourselves to the density  $\rho = 1$ .

### A. Commensurate structures

One of the characteristics of adsorption on solid surfaces is the possibility of formation of commensurate layers. The radial pair distribution function  $g(r)$  is a useful tool to investigate this property. The atomic distances of a two dimensional ideal commensurate structure are easily calculated. We computed  $g(r)$  of the heavy noble gases on the graphene substrate and compared our results with the ideal structures. Typical examples of our results are shown in Fig. 4. For the commensurate layers, the radial pair distribution function presents peaks in good agreement with a commensurate lattice for a wide range of temperatures that go almost to the melting temperature. The Ne adlayer shows this behavior, in Fig. 4 (a) at  $\rho = 1.71$  and  $T = 10$  K, a temperature well below melting  $T_m = 25.5$  K, we can see that the system is in a  $\sqrt{7} \times \sqrt{7}$  superlattice. In the following sections we will discuss in detail how the melting temperatures were computed. As the temperature increases towards the melting temperature, in general the peaks broaden. On the other hand, for non-commensurate lattices of the adlayer with respect to the graphene substrate, the atoms are not found preferentially at distances compatible with the commensurate structure for any considered temperature or density, as we show in Fig. 4 (b) for the Ar adlayer.

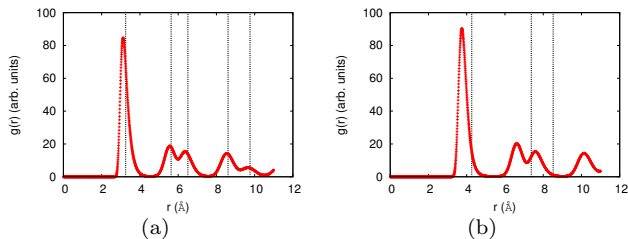


FIG. 4. (Color online) Radial pair distribution functions for Ne atoms at  $T = 10$  K and  $\rho = 1.71$  (a), and for the Ar adlayer at  $\rho = 1$  and  $T = 40$  K (b). The dashed lines correspond to the neighbors distances of atoms in the ideal sites of the commensurate lattices,  $\sqrt{7} \times \sqrt{7}$  (a) and  $\sqrt{3} \times \sqrt{3}$  (b).

We also analyzed the spatial distribution of rare-gas atoms over the graphene sheet by accumulation of a two-dimensional histogram in a grid of the  $xy$  plane over the unit cells of the system depicted in Fig. 3. The results for the two-dimensional histogram of krypton atoms at  $\rho = 1$  and  $T = 100$  K are presented in Fig. 5. As we see, the most probable locations of the Kr atoms are the lattice sites of the  $\sqrt{3} \times \sqrt{3}$  structure. Further evidence to support our claim that Kr atoms form a commensurate adlayer comes from a plot of  $g(r)$ . It shows peaks in agreement with nearest neighbors distances of the ideal commensurate structure in a fashion similar to what is depicted in Fig. 4 (a). This behavior is observed for tem-

peratures below melting, 107.9 K. At higher temperatures, above melting, the probability of finding a Kr atom over the center of a substrate hexagon is higher, although it can be found in other positions as well.

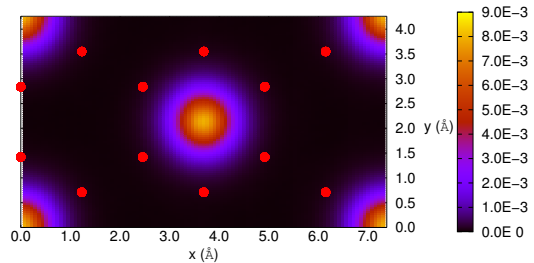


FIG. 5. (Color online) Spatial distribution of Kr atoms over a  $\sqrt{3} \times \sqrt{3}$  cell below melting. The red dots represent the ideal positions of the carbon atoms.

By calculating the radial pair distribution function of atoms in adlayers of Ar, Xe and Rn we found no evidence of commensurate structures with the substrate, even at low temperatures. Nevertheless, the probability of finding one adatom over the center of a substrate hexagon is still larger than in other locations. On top of the carbon atoms were the locations where atoms of the noble gases were found with lowest probability.

### B. Adlayer Specific Heat

The specific heat  $c_v$  is a thermodynamical quantity of both experimental and theoretical interest. It is computed by considering the fluctuations of the average internal energy  $\langle \delta E^2 \rangle_{NVT}$  of the adatoms

$$c_v = \frac{\langle \delta E^2 \rangle_{NVT}}{N_X k_B T^2}, \quad (9)$$

in the canonical ensemble.

The specific heat as a function of the temperature for Ar at  $\rho = 1.08$  that we have calculated is shown in Fig. 6. The behavior of the specific heat for the other noble gases and densities is qualitatively the same. The peak temperature and its characteristic width were determined by fitting to the computed points a curve of the Lorentzian form,

$$c_v(T) = \frac{a}{\pi \gamma \left[ 1 + \left( \frac{T - T_0}{\gamma} \right)^2 \right]} + b, \quad (10)$$

where  $T_0$  is the location of the peak,  $2\gamma$  is its FWHM,  $a$  is related to the area of the curve and  $b$  is a  $y$ -shift. We carried out this procedure to the other rare-gases and densities; the results are summarized in Table III.

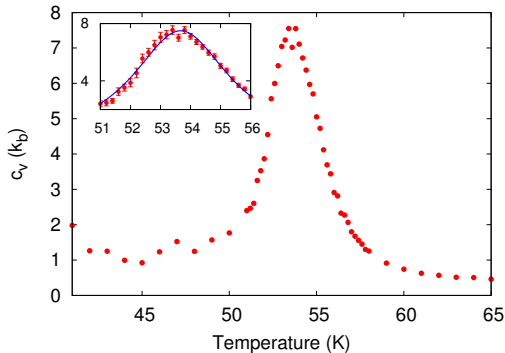


FIG. 6. (Color online) The specific heat of Ar as a function of the temperature for  $\rho = 1.08$ . The region of the peak is magnified in the inset together with the errorbars, the solid line is a function of the Lorentzian form fitted to the results

TABLE III. Temperature and width of the specific heat peak for the given noble gases and densities.

	$\rho$	$T_0$ (K)	FWHM (K)
<b>Ne</b>	1.00	$15.7 \pm 0.1$	$1.9 \pm 0.2$
	1.71	$35.6 \pm 0.2$	$8.3 \pm 0.8$
<b>Ar</b>	0.38	$53.6 \pm 0.2$	$8.6 \pm 0.7$
	0.73	$54.4 \pm 0.1$	$3.7 \pm 0.3$
	1.00	$55.1 \pm 0.1$	$3.9 \pm 0.3$
	1.08	$53.7 \pm 0.1$	$4.0 \pm 0.2$
<b>Kr</b>	1.00	$107.4 \pm 0.2$	$6.5 \pm 1.2$
<b>Xe</b>	1.00	$134.3 \pm 0.5$	$7.9 \pm 1.3$
<b>Rn</b>	1.00	$188.9 \pm 1.6$	$41.0 \pm 8.9$

The temperatures of the specific heat peaks increase with the atomic number as we can see at the density  $\rho = 1$ . Additionally, we observe an enlargement of their characteristic widths. These properties are consistent with the bulk properties of these systems.

It is interesting to compare the specific heat peaks of Ar adlayers at different densities. The temperature  $T_0$  of the peak has its maximum value at the density  $\rho = 1$ . This behavior might be credited to the effects of the graphene substrate that are more evenly distributed through the adatoms. Although the Ar atoms of the adlayer are not preferentially found in the ideal commensurate lattice, the substrate favors the expansion of the adlayer towards the  $\sqrt{3} \times \sqrt{3}$  structure. If we consider the statistic uncertainty of the specific heat peak, we possibly could include in our analysis the system at the density  $\rho = 0.38$ . However, because of size effects, we chose not to do this. At this low density we have found that the adlayer forms islands where the proportion of atoms in the border to those inside are substantial. This is a situation that might cause deviations in the observed trend as we can see in the obtained FWHM.

### C. Melting

The melting of the adlayers is related to the loss of sixfold symmetry that is present in the solid phases of these systems. The study of their melting can be done by following the evolution with temperature of an order parameter related to the sixfold symmetry. For this purpose we introduce the order parameter

$$\Psi_6 = \frac{1}{N_B} \left\langle \left| \sum_{j,k_j}^N \exp(6i\Phi_{jk_j}) \right| \right\rangle, \quad (11)$$

where  $\Phi_{jk_j}$  is the angle between the projections in the  $xy$  plane of the relative position of atom  $j$  and its nearest neighbors  $k_j$  with respect to a fixed axis, e.g., the  $x$ -axis in this plane, and  $N_B$  is the number of bonds used in the calculation. The sum on  $j$  extends over all noble gas atoms. The brackets indicate a thermal average. If the adlayer possesses six-fold symmetry, as a triangular lattice does,  $\Psi_6 = 1$ . For an isotropic fluid,  $\Psi_6$  is zero. Moreover, the loss of the sixfold symmetry can be characterized by a peak in the susceptibility  $\chi_6$  of  $\Psi_6$  given by

$$\chi_6 = \frac{\langle \Psi_6^2 \rangle - \langle \Psi_6 \rangle^2}{T}. \quad (12)$$

The order parameter  $\Psi_6$  and its susceptibility  $\chi_6$  for Ar at  $\rho = 1.08$  is shown in Fig. 7. The order parameter is near unity for low temperatures and drops sharply when the melting occurs. The susceptibility peaks near the transition temperature. We have observed a similar behavior at other densities for this system and for the others rare-gases adlayers as well.

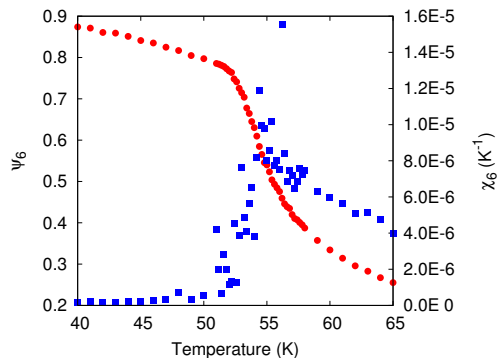


FIG. 7. (Color online) Order parameter (circles) and susceptibility (squares) for Ar at  $\rho = 1.08$  as a function of the temperature.

The points of the susceptibility  $\chi_6$  were fitted to a function of the Lorentzian form. We interpret the fitted parameter  $T_0$  of Eq. (10), as the melting temperature  $T_m$ . Our results are presented in Table IV. If we compare different systems at the same density  $\rho = 1$ , the melting temperature and the Lorentzian FWHM increase with the atomic number. Specifically for the Ar adlayers we

TABLE IV. Melting temperature and characteristic width for various noble gases and densities.

	$\rho$	$T_m$ (K)	FWHM (K)
<b>Ne</b>	1.00	$15.9 \pm 0.1$	$1.3 \pm 0.2$
	1.71	$25.5 \pm 0.2$	$9.5 \pm 1.5$
<b>Ar</b>	0.38	$53.9 \pm 0.1$	$8.2 \pm 1.2$
	0.73	$55.2 \pm 0.1$	$4.0 \pm 0.8$
	1.00	$56.0 \pm 0.1$	$3.1 \pm 0.5$
	1.08	$55.5 \pm 0.2$	$5.2 \pm 2.0$
<b>Kr</b>	1.00	$107.9 \pm 0.2$	$4.2 \pm 0.6$
<b>Xe</b>	1.00	$175.3 \pm 0.4$	$10.0 \pm 1.5$
<b>Rn</b>	1.00	$234.9 \pm 1.0$	$20.0 \pm 5.2$

can analyze the melting temperature as a function of the density. This quantity has a maximum at  $\rho = 1$ , and the behavior as a function of the density might be attributed to the substrate. Like what we observed for the specific heat, the substrate drives in a more effective way an evenly distribution of the adlayer atoms towards a  $\sqrt{3} \times \sqrt{3}$  structure.

#### D. Nearest neighbor distance

An estimate of the nearest neighbor distance  $\langle a \rangle$  can be obtained from the pair distribution function  $g(r)$ . The behavior of  $\langle a \rangle$  as a function of the temperature can be quite different for the various densities and rare-gases studied. In fact, we have observed three different ones. It can smoothly increase with temperature, which is the case of Ne at  $\rho = 1$  and of Ar at all considered densities. For the two commensurate layers that we have observed in our calculations,  $\sqrt{7} \times \sqrt{7}$  Ne and  $\sqrt{3} \times \sqrt{3}$  Kr, the nearest-neighbor (NN) distance presents a minimum near the melting temperature. Finally, the NN distance  $\langle a \rangle$  can sharply increase as the temperature approaches the specific heat peak in a way that can be associated with the promotion of adatoms to a second layer, as we have observed for Xe and Rn at  $\rho = 1$ .

We begin by analyzing the mean NN distance of Ar adatoms at various densities as a function of the temperature presented in Fig. 8. At low densities, *i.e.*,  $\rho = 0.38$  and  $0.73$ , we observe a NN distance that increases with temperature. This behavior can be explained by the fact that, at low densities, the adlayer does not cover entirely the graphene substrate. However, with the increase of thermal energy, the atoms become more free to move, and will occupy more evenly the available space. At density  $\rho = 1.08$  and for the high range of temperatures we have considered in our calculations, we see that the NN distance saturates. At the density  $\rho = 1$  it seems that the mean value of the NN distance is almost reaching a saturation regime at this same range of temperatures. This situation can be explained if we consider the Helmholtz free energy  $F$  (we are working within the canonical *en-*

*semble*),

$$F = E - TS, \quad (13)$$

where  $E$  is the internal energy and  $S$  is the entropy. For low temperatures, the free energy is dominated by the internal energy  $E$ , and the layer can expand as the temperature rises. Since the term  $TS$  is significant at higher temperatures, disorder in the layer is energetically favored instead of its expansion. This situation of nearly constant  $\langle a \rangle$  would persist until second layer promotion would be thermally activated<sup>5</sup>. At the two highest densities of the Ar adlayers we have observed a puzzling feature, for a small range of temperatures below the specific heat peak, which is the approximated constant value of  $\langle a \rangle$ . This behavior can not be associated with the promotion of atoms to a second layer as we will see in Sec. III E. For Ne at  $\rho = 1$  the NN distance increases with the temperature, qualitatively displaying a behavior that resembles the one of Ar at  $\rho = 0.78$ .

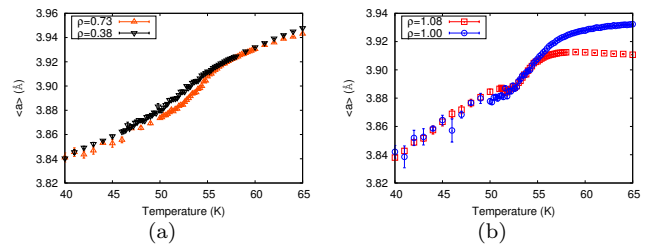


FIG. 8. (Color online) Nearest neighbor distance as a function of the temperature for Ar at the given densities.

The second behavior we have observed is typical of adlayers commensurate with a substrate, where the nearest neighbor distance initially decreases with temperature before increasing as expected. In our calculations, Ne at  $\rho = 1.71$  and Kr at  $\rho = 1$  have presented this behavior. For Kr we show in Fig. 9 a plot of the average NN distance as a function of temperature. The minimum of the nearest neighbor distance happens about the melting temperature, and the FWHM of the fitted curve to  $\chi_6$  encompasses the change between negative and positive slopes. Above  $T_0$  the liquid expands, as expected. For the Ne adatoms, as the temperature increases they gain sufficient energy to overcome the substrate potential and get closer together. On the other hand, the Kr adatoms feel more the substrate, as the temperature increases up to melting, and the NN distance decreases.

Finally, a third behavior is observed for adsorbed layers of Xe and Rn. The NN distance as a function of temperature for Xe at  $\rho = 1$  is shown in Fig. 10. The abrupt change of this quantity happens near the specific heat peak, as we can see in the figure, and a substantial part of the step variation in the NN distance occurs within a temperature range given by the FWHM of this peak. The promotion of Xe atoms to a second layer is responsible for the observed behavior. The Rn adlayer at

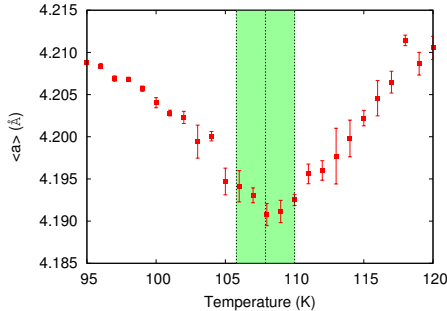


FIG. 9. (Color online) Nearest neighbor distance of Kr atoms in adlayers at  $\rho = 1$ . The centered dotted vertical line shows the melting temperature  $T_0 = 107.9$  K. The region between the external dotted vertical lines correspond to the FWHM of the melting peak.

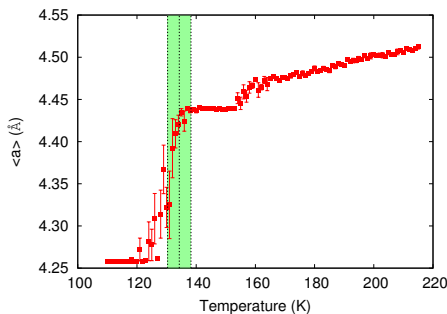


FIG. 10. (Color online) First neighbor distance as a function of the temperature for Xe at  $\rho = 1$ . The dotted vertical lines show the FWHM temperature region of the specific heat peak indicated by a dotted vertical line at  $T_0 = 134.3$  K

$\rho = 1$  presents similar features to those we have described above.

### E. Distance from the substrate

The average perpendicular distance  $\langle z \rangle$  from the adatoms to the substrate plane was computed by accumulating the  $z$  coordinates of the adatoms during the simulations. This quantity for Ar adlayers at  $\rho = 0.38, 0.73, 1$  and  $1.08$  is displayed in Fig. 11. The expected behavior of the distance  $\langle z \rangle$  from the substrate, namely, its increase with density is observed at low and high temperatures. However near the melting temperature and the specific heat peak deviations occur. For example, at  $\rho = 1$ ,  $\langle z \rangle$  presents its highest value. In this work we have no evidence of a second adlayer formation of Ar atoms.

Adlayers of Ne present similar characteristics to those of Ar. However for the adlayer at density  $\rho = 1$  the adatoms are always closer to the substrate than those at  $\rho = 1.71$ , most probably due to a much smaller coverage in this case. On the other hand, the Kr adlayer presents a fascinating behavior that can be seen in Fig 12, the distance from substrate has an inflection point, which

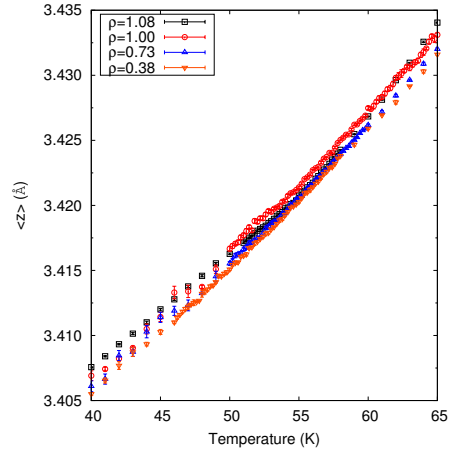


FIG. 11. (Color online) Distance from the substrate as a function of the temperature for Ar adlayers at the given densities.

coincides with the specific heat peak temperature.

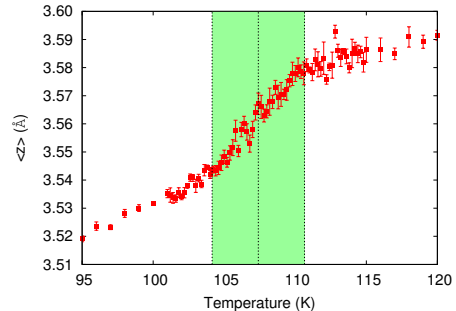


FIG. 12. (Color online) Average distance from the Kr adlayer to the graphene substrate as a function of the temperature at density  $\rho = 1$ . The vertical dotted lines show the specific heat peak at  $T_0 = 107.4$  K and the temperature region of the FWHM of this peak.

Finally we analyze the Xe adlayer, where there was the formation of a second adsorbed layer as we can see in Fig 13. In the second adlayer the distance  $\langle z \rangle$  is approximately constant for temperatures above  $T_0$ , the temperature of the specific heat peak. It is interesting to note that in the first adlayer the distance  $\langle z \rangle$  continues to increase smoothly even after the second layer becomes stable.

## IV. DISCUSSION AND CONCLUSIONS

One of the contributions of our work on adsorption of noble gases on graphene is the evidences of commensurate adlayers, which depend strongly on the symmetry of the exposed substrate surface. Since graphene and graphite present the same surface, we looked for the well-known commensurate structures previously observed on graphite<sup>3</sup>. We observed two commensurate structures at low temperatures; the Ne adlayer forms a  $\sqrt{7} \times \sqrt{7}$

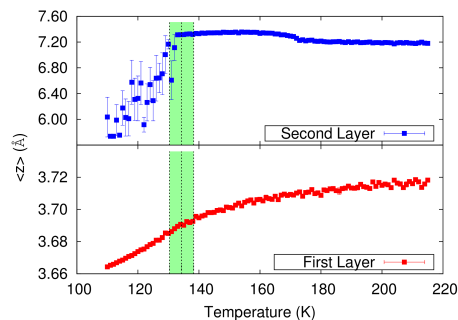


FIG. 13. (Color online) Distance from the substrate as a function of the temperature for Xe adlayers at  $\rho = 1$ . The dotted vertical lines corresponds to the specific heat peak  $T_0 = 134.3$  K and also delimits its corresponding FWHM. Note that the  $y$ -scale differs between the different layers.

lattice and Kr adatoms are found in the  $\sqrt{3} \times \sqrt{3}$  structure. Although both substrates share many aspects, this is remarkable because graphene is a much less attractive substrate than graphite, and we could not know if these structures would be found *a priori*. However, we were not able to observe a commensurate phase for Xe adlayers like it was observed for this system in a graphite substrate.

The understanding of the specific heat peaks and the melting transition can be attained by considering the influence of the substrate on the adlayer. The specific heat is a quantity of thermodynamical interest that can be measured in experiments with relatively simple apparatus. Its peaks can hint the order of the melting transition. For graphite substrates, all heavy noble gases present continuous melting, with the possible exception of Ar due to a narrow peak in the specific heat (at the shoulder of a broad peak at  $\sim 50$  K). We determined the position and width of the peaks for the heavy rare-gases at various densities, and we only found evidences of continuous melting, due to the broad FWHM observed for these peaks.

The melting, and its sixfold symmetry, was also investigated. We introduced an order parameter and determined the melting temperature using its susceptibility. The melting temperature, along with the FWHM, indicates a temperature range in which we have solid-liquid coexistence. Moreover, the probability of finding one noble gas atom over the center of a carbon hexagon is higher than in other positions. This might explain the deviations found for Ar at  $\rho = 1.08$  in the specific heat and also in the melting transition. Apparently, because of the energy costs, the increase of the density slightly above  $\rho = 1$  allows a more frequent occupation of sites other than the center of the hexagons, which facilitates the melting transition.

The behaviors of the different adlayer are very rich. In addition to the arguments we already gave to explain our observations we can advance some tentative ideas based on the interplay between the mutual interaction of the

adlayer atoms and their interaction with the substrate and also by considering the van der Waals radius of these interactions. The pair interaction noble-gas-noble-gas is stronger than noble-gas-carbon, and the former is enough to prevent the formation of the commensurate lattice in most cases.

For Ar atoms the minima of both the mutual interaction and the one with the substrate occurs approximately at the same pair separation. The van der Waals radius for both interactions are also about of the same value. These characteristics seem enough to explain the observed behavior of the NN distance, it increases with temperature. At density  $\rho = 1$  the Ne atoms also display the above characteristic despite of different van der Waals radius for the Ne-Ne and Ne-C interactions. Probably the observed behavior can be explained by a very similar value of the minima of these interactions.

Adlayers that are commensurate initially show a decrease with temperature for the NN distance. For the Ne atoms we may attribute this to both the high coverage this system has with respect to the substrate and a slightly strong minimum Ne-Ne interaction. On the other hand, as the Kr atoms gain thermal energy they become less affected by the minimum of the Kr-Kr interaction and prefer to stay close to the minimum of the Kr-C interaction which has also a smallest van der Waals radius. In general, it seems the systems preference is to chose a state where the van der Waals radius is minimum.

The third behavior we have observed, the promotion of Xe and Rn atoms at certain temperatures to a second layer may be due to the much stronger mutual interaction these atoms have among themselves than with the substrate. Although as the temperature increases the atoms would prefer to go more near the substrate interaction minima, the mutual attraction is so intense that the energy cost makes preferable the promotion of the adatoms to the second layer.

The nearest neighbor distance is smaller than the one reported for the same noble gases on graphite, which is a consequence of graphene being a less attractive substrate. For Ne adlayers on graphite the experimental value of  $(3.25 \pm 0.02)$  Å at  $T = 1.5$  K and  $\rho = 1.71$  has been reported<sup>17</sup>, which is larger than all values we observed in the range  $10 \leq T \leq 50$  K. The experimental value<sup>18</sup> for the nearest neighbor distance for Ar/graphite at  $\rho = 1$  and  $T = 49.7$  K is 3.97 Å, also larger than the value we observe for graphene substrates. Monte Carlo simulations of Ar/graphite<sup>5</sup> also report larger nearest neighbor distances for  $\rho = 0.39$  and 0.71. The system Xe/graphite exhibits a nearest neighbor spacing<sup>19</sup> of 4.59 Å at  $\rho = 1$  and  $T = 97$  K, also larger than our values. Moreover, the distance from the substrate also appears to be larger for noble gases on graphite. Simulations for Ar adlayers<sup>5</sup> show their distance varying between 3.42 to 3.49 Å at  $\rho = 1.14$  in the temperature range of 30 to 80 K, which is larger than our values.

We also computed the average distance between the adlayer and the substrate. As we have already discussed,



it is possible to relate the behavior of this quantity directly to the specific heat peaks or the melting transition.

Future calculations will include a more detailed study of the phase transitions, which can lead to the construction of phase diagrams. We also intend to include more accurate potentials for the interaction between the noble gases atoms and the graphene layer, such as the substrate-mediated (McLachlan) potential<sup>20</sup>.

This work enlarges the body of knowledge found in the literature about noble gases adsorbed on carbon substrates. To the best of our knowledge, experimental data is not available for the noble-gas/graphene system. We

hope that this study can motivate experiments to increase our understanding of these systems.

## ACKNOWLEDGMENTS

We gratefully acknowledge support from the Brazilian agency São Paulo Research Foundation (FAPESP), grants 2012/24195-2 and 2010/10072-0. The calculations were performed at CCJDR-IFGW-UNICAMP and CENAPAD-SP (project 139).

---

\* lucas.madeira@asu.edu

- <sup>1</sup> L. W. Bruch, R. D. Diehl, and J. A. Venables, *Rev. Mod. Phys.* **79**, 1381 (2007).
- <sup>2</sup> G. Huff and J. Dash, *Journal of Low Temperature Physics* **24**, 155 (1976).
- <sup>3</sup> L. Bruch, M. Cole, and E. Zaremba, *Physical Adsorption: Forces and Phenomena*, International series of monographs on chemistry (Clarendon Press, 1997).
- <sup>4</sup> A. D. Migone, Z. R. Li, and M. H. W. Chan, *Phys. Rev. Lett.* **53**, 810 (1984).
- <sup>5</sup> E. Flenner and R. D. Etters, *Phys. Rev. B* **73**, 125419 (2006).
- <sup>6</sup> V. Pershina, A. Borschevsky, E. Eliav, and U. Kaldor, *The Journal of Chemical Physics* **129**, 144106 (2008).
- <sup>7</sup> J. Tersoff, *Phys. Rev. B* **37**, 6991 (1988).
- <sup>8</sup> J. Tersoff, *Phys. Rev. B* **39**, 5566 (1989).
- <sup>9</sup> J. Tersoff, *Phys. Rev. B* **41**, 3248 (1990).
- <sup>10</sup> R. A. Aziz and M. Slaman, *Chemical Physics* **130**, 187 (1989).
- <sup>11</sup> R. A. Aziz and M. Slaman, *Molecular Physics* **58**, 679 (1986).
- <sup>12</sup> R. A. Aziz and M. Slaman, *Molecular Physics* **57**, 825 (1986).
- <sup>13</sup> R. A. Aziz, *The Journal of Chemical Physics* **99**, 4518 (1993).
- <sup>14</sup> K. T. Tang and J. P. Toennies, *The Journal of Chemical Physics* **118**, 4976 (2003).
- <sup>15</sup> N. Inui, K. Mochiji, and K. Moritani, *Nanotechnology* **19**, 505501 (2008).
- <sup>16</sup> S. Plimpton, *J Comp Phys* **117**, 1 (1995), <http://lammps.sandia.gov>.
- <sup>17</sup> C. Tiby, H. Wiechert, and H. Lauter, *Surface Science* **119**, 21 (1982).
- <sup>18</sup> K. L. D'Amico, J. Bohr, D. E. Moncton, and D. Gibbs, *Phys. Rev. B* **41**, 4368 (1990).
- <sup>19</sup> W. J. Nuttall, K. P. Fahey, M. J. Young, B. Keimer, R. J. Birgeneau, and H. Suematsu, *Journal of Physics: Condensed Matter* **5**, 8159 (1993).
- <sup>20</sup> L. W. Bruch, M. W. Cole, and H.-Y. Kim, *Journal of Physics: Condensed Matter* **22**, 304001 (2010).